CONF-891208--28

PNL-SA-16718

PNL-SA--16718

DE90 004671

NUMERICAL PREDICTIONS OF LOCAL ENTROPY GENERATION FOR AN IMPINGING JET

M. D. White
M. K. Drost

April 1989

Presented at the
ASME Winter Annual Meeting
San Francisco, CA.
December 10-15, 1989

Work supported by
the U.S. Department of Energy
under Contract DE-AC06-76RLO 1830

Pacific Northwest Laboratory
Richland, Washington 99352

DISCLAIMER

This report was prepared as an account of work sponsored by an agency of the United States Government. Neither the United States Government nor any agency thereof, nor any of their employees, makes any warranty, express or implied, or assumes any legal liability or responsibility for the accuracy, completeness, or usefulness of any information, apparatus, product, or process disclosed, or represents that its use would not infringe privately owned rights. Reference herein to any specific commercial product, process, or service by trade name, trademark, manufacturer, or otherwise does not necessarily constitute or imply its endorsement, recommendation, or favoring by the United States Government or any agency thereof. The views and opinions of authors expressed herein do not necessarily state or reflect those of the United States Government or any agency thereof.

DISTRIBUTION OF THIS DOCUMENT IS UNLIMITED

MASTER

DISCLAIMER

This report was prepared as an account of work sponsored by an agency of the United States Government. Neither the United States Government nor any agency thereof, nor any of their employees, makes any warranty, express or implied, or assumes any legal liability or responsibility for the accuracy, completeness, or usefulness of any information, apparatus, product, or process disclosed, or represents that its use would not infringe privately owned rights. Reference herein to any specific commercial product, process, or service by trade name, trademark, manufacturer, or otherwise does not necessarily constitute or imply its endorsement, recommendation, or favoring by the United States Government or any agency thereof. The views and opinions of authors expressed herein do not necessarily state or reflect those of the United States Government or any agency thereof.

DISCLAIMER

Portions of this document may be illegible in electronic image products. Images are produced from the best available original document.

Numerical Predictions of Local Entropy Generation for an Impinging Jet

Dr. Mark D. White
Research Engineer
Pacific Northwest Laboratory[a]

Dr. M. Kevin Drost
Senior Research Engineer
Pacific Northwest Laboratory

ABSTRACT

Predictions of local volumetric entropy generation rates were made numerically for the convective heat transfer problems of a fluid jet impinging on isothermal and constant heat flux surfaces. The solution technique yielded a scalar field of volumetric entropy generation rates that extends over the fluid domain. For isotropic and Newtonian fluids local entropy generation rates, that stem from the irreversible phenomena of heat transfer across a finite temperature difference and viscous fluid flow, may be computed from fields of temperature, local temperature gradients, and the local viscous dissipation function. TEMPEST, a three-dimensional, time-dependent computer program for hydrothermal analysis was used to compute numerical solutions to the Navier-Stokes balance equations of mass, momentum, and energy for the fluid domain encompassing the impinging jet. The results from these numerical solutions included the local values of temperature and velocity that are required to compute entropy generation rates. Translation of scalar temperature and vector velocity fields into scalar fields of volumetric entropy generation was effected through a recently added subroutine appropriately called ENTROPY. Before analyzing the impinging jet problem the TEMPEST code configured with the ENTROPY subroutine was successfully validated against convective heat transfer problems for which analytical solutions were known. The primary points of interest for this problem were to investigate the surface heat transfer rates as a function of inlet jet velocities, and the apportionment between viscous and thermal source entropy generation. The problem investigated was restricted to two-dimensional slot jet flow with two fluids, helium and glycerin.

INTRODUCTION

Second Law analysis techniques have been widely used to evaluate the sources of irreversibilities in components and systems of components but the evaluation of local

---

[a] Operated by Battelle Memorial Institute for the U.S. Department of Energy Under Contract DE-AC06-76RLO 1830.

sources of irreversibilities in thermal processes has received limited attention. While procedures for evaluating local entropy generation were developed in 1979 (Bejan 1979a, 1982), applications have been limited to fluid flows with analytical solutions for the velocity and temperature fields. A recent review of Second Law techniques applicable to basic research in the thermal sciences recommended that entropy generation calculations be included in computational fluid dynamics (CFD) codes to allow the evaluation of local entropy generation in more complicated thermal phenomena (Drost and Zaworski 1988). The research documented in the present paper consisted of the incorporation of entropy generation relations in an existing CFD code and then using the code to evaluate local entropy generation in an impinging jet. The specific objectives of the research include:

- Incorporate calculations for local entropy generation in an existing CFD code.
- Benchmark the entropy generation calculations by comparison of numerical results with analytical calculations for laminar pipe flow.
- Investigate the sources and distribution of entropy generation in an impinging jet for a range of fluids and fluid velocities.

The application of partial differential equations describing local entropy generation to convecting fluids was initially developed by Bejan (1979a) and was used to evaluate entropy generation in fluid flows for which analytical solutions of the velocity and temperature fields were available (Bejan 1979a, 1982). Bejan also evaluated local entropy generation in internal and external flows using a lumped parameter approach (Bejan 1979b, 1982) and investigated local entropy generation in insulation systems. Dunbar (1982) has applied a one-dimensional lumped parameter analysis to the evaluation of a fuel cell while Hutchinson and Lyke (1987) have used a similar approach to investigate irreversibilities in a Stirling engine regenerator. Two recent papers have evaluated local entropy generation in heat exchangers by applying a lumped parameter analysis (Liang and Kuehn 1988, El-Sayed 1988). Whereas, Argrow et al. (1987) have suggested calculating natural entropy generation as a method of evaluating the importance of numerical entropy generation. A literature review did not identify any previous studies that actually incorporated entropy generation relationships in a CFD code and then used the code to evaluate a important thermodynamic process.

One goal of Second Law analysis is to identify and minimize the thermodynamic irreversibilities associated with a process or component. It can be shown that the minimization of entropy generation results in irreversibility minimization (Bejan 1982). For an isotropic convecting fluid, entropy generation is given by Equation (1) for three dimensional rectangular coordinates (Bejan 1979a, 1982):

$$\dot{S}'''_{gen} = \frac{\kappa}{T^2}\left[\left(\frac{\partial T}{\partial x}\right)^2 + \left(\frac{\partial T}{\partial y}\right)^2 + \left(\frac{\partial T}{\partial z}\right)^2\right] + \frac{\varepsilon}{T}\left\{2\left[\left(\frac{\partial u}{\partial x}\right)^2 + \left(\frac{\partial v}{\partial y}\right)^2 + \left(\frac{\partial w}{\partial z}\right)^2\right] + \left(\frac{\partial u}{\partial y} + \frac{\partial v}{\partial x}\right)^2 + \left(\frac{\partial u}{\partial z} + \frac{\partial w}{\partial x}\right)^2 + \left(\frac{\partial v}{\partial z} + \frac{\partial w}{\partial y}\right)^2\right\} \quad (1)$$

The first bracketed term on the left hand side of Equation (1) is the entropy generation due to heat transfer across a finite temperature difference, whereas the second and third bracketed terms are the local entropy generation due to viscous dissipation. When analytical expressions are available for the temperature and velocity fields, Equation (1) can be evaluated to yield the local entropy generation. Total entropy generation can be determined by integrating Equation (1) over the region of interest. Most practical problems are sufficiently complex that analytical solutions do not exit. In this case, a CFD code can be used to predict the velocity and temperature fields. This information can then be used to numerically calculate entropy generation. The details of incorporating Equation (1) in an existing CFD code and benchmarking studies are discussed below.

The CFD code with numerical entropy generation calculations was then used to evaluate impingement heat transfer where a slot jet is impinging on a hot wall. The problem is shown in Figure 1. The goal of the study was to evaluate the source and distribution of entropy generation in the jet. Impingement heat transfer has been used for turbine blade cooling, cooling of electronic components, and for air heating in solar thermal power applications. Understanding the structure of entropy generation in this process should be of direct utility to heat transfer engineers. Helium and glycerin were evaluated as heat transfer fluids. While helium is often used as a heat transfer fluid, glycerin was included as a limiting case where viscous dissipation becomes the dominant source of entropy generation, even at low velocities.

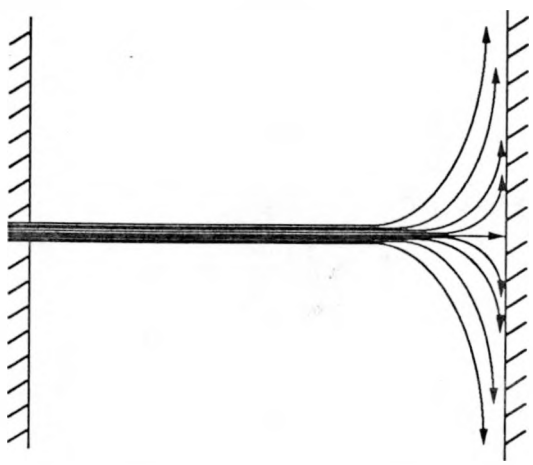

FIGURE 1. Impinging Jet

MODELING METHODOLOGY

The approach to computing local entropy generation rates was based on the equations derived by Bejan (1982) for the irreversibilities associated with viscous flow and heat transfer across a finite temperature difference. Bejan's expression for local entropy generation rate, in Cartesian coordinates, for a Newton fluid and isotropic medium appears as in Equation (1); where $\kappa = k + k_T$ and $\varepsilon = \mu + \mu_T$. Expressed in the above form Equation (1) is valid for both laminar and turbulent flow; where the effective thermal conductivity equals the sum of the molecular thermal conductivity and the eddy thermal conductivity, and the effective viscosity equals the sum of the molecular viscosity and the eddy diffusivity. Local entropy generation rates are, therefore, dependent on the local spatial gradients of temperature and velocity and on the absolute local values of temperature, effective thermal conductivity, and viscosity. These quantities were estimated locally within the fluid domain for fluid flow and convective heat transfer problems with the finite-difference based TEMPEST computer code (Trent, Eyler and Budden 1989a,b). The pertinent aspects of the TEMPEST code to the computation of entropy generation for fluid flow and convective heat transfer are described below.

The method for computing local entropy generation was to substitute finite difference formulations for the partial derivative terms of Equation (1), and evaluate the resulting expression after each TEMPEST time advance. The evaluation of the local entropy generation throughout the computational domain was decoupled from computations of the primitive variables of temperature, pressure, velocity, turbulent kinetic energy, and dissipation of turbulent kinetic energy. Conserving the first order accurate finite differencing scheme used in the TEMPEST code, the entropy generation equation was differenced to first order accuracy. The difference expressions for three of the twelve partial differential terms in Equation (1) are expressed below for illustration:

$$\left(\frac{\partial T}{\partial x}\right)^2 = \left\{ \frac{(\Delta x_{i-1} + \Delta x_i) T_{j+1} - (\Delta x_{i+1} + \Delta x_i) T_{i-1} + (\Delta x_{i+1} + \Delta x_{i-1}) T_j}{(\Delta x_{i+1} + \Delta x_i)(\Delta x_{i-1} + \Delta x_i)} \right\}^2 \tag{2}$$

$$\left(\frac{\partial u}{\partial x}\right)^2 = \left(\frac{u_i - u_{i-1}}{\Delta x_i}\right)^2 \tag{3}$$

$$\left(\frac{\partial v}{\partial x}\right)^2 = \left\{ \left[\frac{(\Delta x_{i-1} + \Delta x_i)(v_{i+1,j} + v_{i+1,j-1})}{2(\Delta x_{i+1} + \Delta x_i)(\Delta x_{i-1} + \Delta x_i)} \right] - \left[\frac{(\Delta x_{i+1} + \Delta x_i)(v_{i-1,j} + v_{i-1,j-1})}{2(\Delta x_{i+1} + \Delta x_i)(\Delta x_{i-1} + \Delta x_i)} \right] + \left[\frac{(\Delta x_{i-1} + \Delta x_{i+1})(v_j + v_{j-1})}{2(\Delta x_{i+1} + \Delta x_i)(\Delta x_{i-1} + \Delta x_i)} \right] \right\}^2 \tag{4}$$

The subscripts i and j are indices for the positive x and y Cartesian coordinate directions, respectively. The subscripting convention is to suppress all indices except for those indices that differ from the local cell (i,j,k). The finite difference expression for entropy generation shown below reflects the staggered grid arrangement used in TEMPEST; that is, the scalar variables are cell centered, whereas the velocities are positioned on the cell faces. The u velocity associated with the i,j,k cell is positioned on the face between the i,j,k and i+1,j,k cells. The same indexing logic holds for the y and z Cartesian directions.

TEMPEST, a three-dimensional, time-dependent computer program for hydrothermal analysis generated the velocity and temperature gradients required to compute the local entropy generation rate. Although TEMPEST offers simulation capabilities over a wide realm of hydrothermal problems, only those features germane to the benchmark and demonstration problems will be addressed. TEMPEST solves the three conservation equations governing mass, momentum, and energy, subject to several assumptions and/or restrictions. The subject fluid is modeled as single-phase, incompressible, and Newtonian. The Boussinesq approximation holds, and the heating contribution due to viscous dissipation is eliminated from the energy equation. These assumptions combine to yield a loosely coupled momentum and energy equation through thermodynamic state relationship for simulations where the natural convection contribution is significant.

The turbulent flow conservation equations are time averaged and Reynolds stresses are incorporated through appropriate eddy viscosity models. In the current version of TEMPEST, turbulent flow Reynolds stresses are modeled through an effective viscosity. The Prandtl-Kolmogorov hypothesis is used to relate the effective viscosity to a velocity and a length scale. In this approach, transport equations for the turbulent kinetic energy and the dissipation of turbulent kinetic energy are solved to determine the effective turbulent viscosity. The turbulent viscosity is in turn employed to compute the turbulent (eddy) thermal conductivity.

The TEMPEST solution procedure is a semi-implicit time marching finite-difference procedure with all governing equations solved sequentially. For each time step the momentum equations are solved explicitly and the pressure equations implicitly. Temperature, turbulent kinetic energy, dissipation of turbulent kinetic energy, and other scalar transport equations are solved using an implicit continuation procedure. The solution proceeds in three phases. During the "tilde phase" the three momentum equations are advanced in time to obtain approximations to the velocity field based on previous time step values of the pressure and density field. These tilde velocity fields satisfy the momentum equation, but not necessarily the continuity of mass equation. The implicit phase computes corrections to the velocity and pressure fields such that the adjusted quantities satisfy the continuity equation. With the implicit phase velocities computed, the scalar phase updates (time advances) the values of temperature and other scalar quantities. The solution is advanced step by step in time by continued application of the above three solution phases. For the steady-state solutions of the present work, the concept of time stepping is somewhat false, rather

the solution is brought to steady-state from some arbitrary initial guess through a series of false transients. The calculation of the entropy generation quantities could be considered as part of the scalar phase; however, unlike other scalars such as temperature, turbulent kinetic energy and dissipation of turbulent kinetic energy the entropy generation quantities do not feed back to momentum equation, e.g., gravitational body force and turbulent viscosity. The entropy generation quantities should, therefore, be considered as post scalar phase.

BENCHMARK PROBLEM

The subroutine to compute entropy generation rates, incorporated into TEMPEST, was benchmarked against the analytical solution for the hydrothermal problem of laminar flow in a circular conduit with constant heat flux. The problem was specifically structured such that the contributions to entropy generation were comparable between the viscous dissipation and thermal gradient portions of the entropy generation equation. The characteristics of the entropy generation benchmark involved the flow of 150° C helium at an average velocity of 8.75 m/s, through a circular conduit with a diameter of 0.05 m, with a constant wall heat flux of 45 W/m^2. The properties of helium were held constant for both the analytical and numerical evaluations. The analytical solution for the velocity profile and temperature profile for laminar flow in a circular pipe with a constant wall heat flux may be expressed as (Kays and Crawford 1980):

$$u = 2V\left(1 - \frac{r^2}{r_o^2}\right) \tag{5}$$

$$T = T_o - \frac{\dot{q}_o''}{k}\left(\frac{3}{4}r_o + \frac{r^4}{4r_o^3} - \frac{r^2}{r_o}\right) \tag{6}$$

The local entropy generation rate then follows from the cylindrical form of Equation (1) as:

$$\dot{S}'''_{gen} = \frac{k\left\{\frac{\dot{q}_o''}{k}\left(\frac{r^3}{r_o^3} - 2\frac{r}{r_o}\right)\right\}^2}{\left\{T_o - \frac{\dot{q}_o''}{k}\left(\frac{3}{4}r_o + \frac{r^4}{4r_o^3} - \frac{r^2}{r_o}\right)\right\}^2} + \frac{\mu\left(\frac{-4Vr}{r_o^2}\right)^2}{\left\{T_o - \frac{\dot{q}_o''}{k}\left(\frac{3}{4}r_o + \frac{r^4}{4r_o^3} - \frac{r^2}{r_o}\right)\right\}^2} \tag{7}$$

where the left and right portion of the right-hand side correspond to the entropy generation contributions for the thermal gradients and viscous dissipation, respectively.

The benchmark problem was modeled with TEMPEST in two-dimensional cylindrical coordinates with an axis of symmetry around the conduit center line. An axial conduit length of 36 m was modeled to assure a fully developed flow at the comparison point. The inlet flow and temperature profiles assigned across the conduit radius were uniform and allowed to develop the axial length of the model. Local entropy generation profiles were computed at each of the non-uniformly spaced, radial nodes across the conduit radius at the model effluent. The contributions to local entropy generation due to thermal gradients and viscous dissipation were computed separately and then compared with the analytical solution. The wall temperature used in the analytical solution matched that of the model wall temperature at the conduit effluent. A comparison of local entropy generation across the conduit radius is show in Figure 2.

The comparison demonstrates that both the TEMPEST code and the entropy generation subroutine function as expected for laminar flow. The TEMPEST approach to turbulent flow with the turbulent kinetic energy and dissipation of turbulent kinetic energy (k-e) model has been thoroughly benchmarked for a variety of applications. The entropy subroutine was verified for turbulent flow through independent calculations of local entropy generation for established turbulent flow fields with convective heat transfer.

IMPINGING JET PROBLEM

To demonstrate the utility of computing local entropy generation for convective heat transfer, a problem was created that was capable of producing comparable levels of entropy generation between the thermal and viscous components. With the appropriate choice of the fluid, Prandtl number, jet Reynolds number and surface Nusselt number, a jet of lower temperature fluid impinging on an elevated temperature isothermal wall can develop complex velocity and temperature fields with interesting entropy generation regions. The impinging jet problem provides the opportunity for viscous source entropy generation in distinct areas of the model because of the strong shears that develop near the jet inlet and along the compression wall. With surface heat transfer limited to the isothermal wall, the thermal source entropy generation will primarily occur near the wall with some turbulent mixing away from the wall producing local thermal gradients. Although TEMPEST and the associated entropy subroutine are fully transient and three-dimensional, the impinging jet problem was limited to a steady-state and two-dimensions.

The physical arrangement and noding scheme for the impinging jet problem are shown in Figure 3. A fluid jet enters the computational domain in the lower corner of the left vertical boundary as a uniform specified velocity. In the horizontal direction the computational domain is bounded by two vertical walls; the left wall being an adiabatic, no slip surface and the right wall being either an isothermal or constant heat flux, no slip surface. The upper horizontal surface is an unspecified outflow/inflow boundary for which the conditions are computed. The modeled problem is actually double the size depicted with a line of symmetry position on the center line of the jet

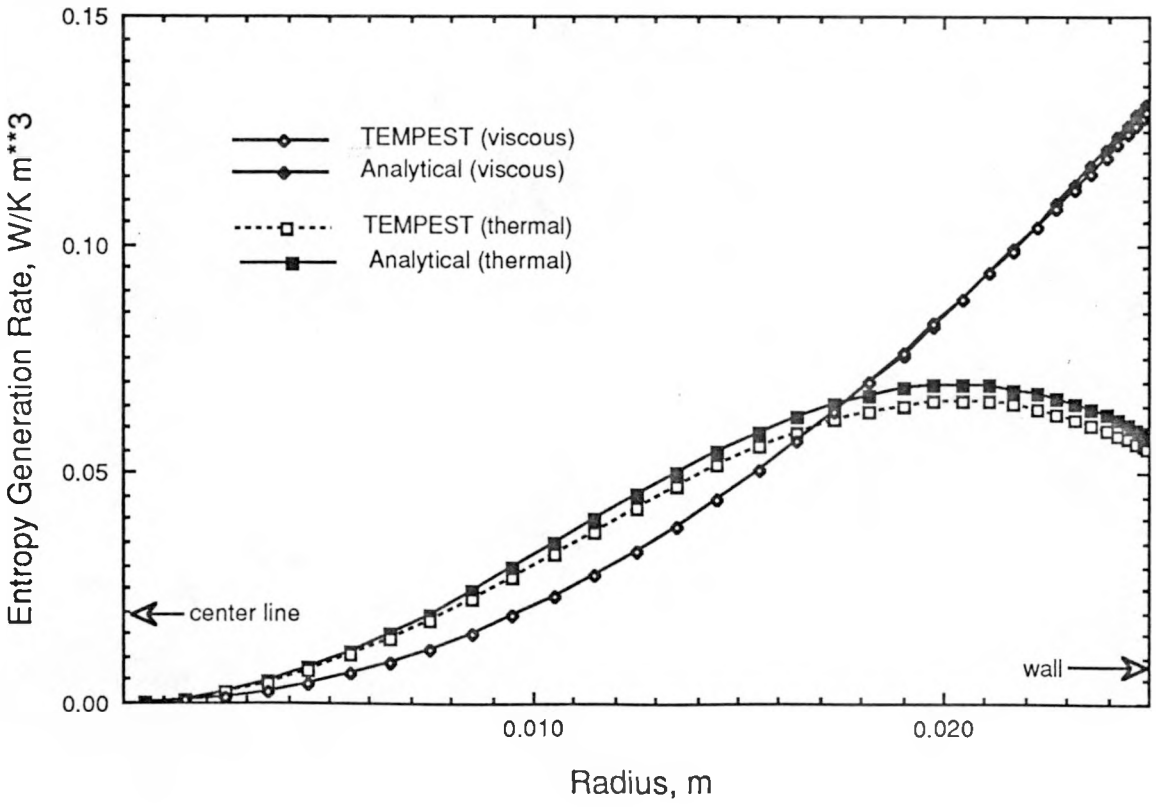

FIGURE 2. Entropy Generation for Laminar Flow with Constant Heat Flux

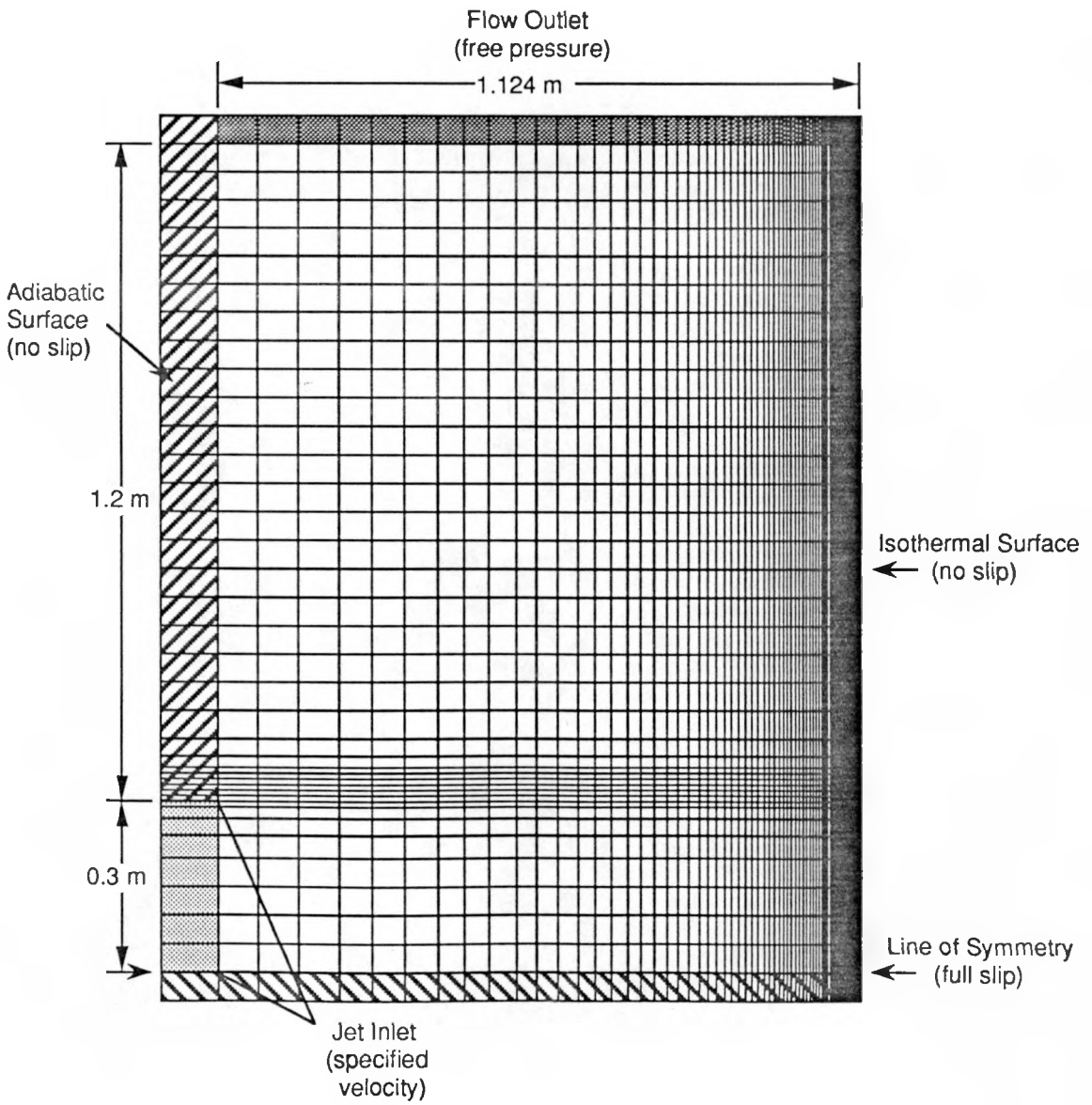

FIGURE 3. Computational Grid for the Impinging Jet Problem

inlet. The lower horizontal boundary has, therefore, a rigid free-slip flow condition, with an adiabatic surface. The inlet jet spans a surface area of 0.3 m^2/m, whereas, the flow outlet covers the entire upper horizontal surface 1.124 m^2/m. Vertically the computational domain was arbitrarily limited to a 1.5 m length.

The computational noding scheme was a 60 x 40 Cartesian grid with variable node spacing. The horizontal node spacing varied between 0.0711 m and 0.001 m, and the vertical node spacing varied between 0.05 m and 0.01 m. The high aspect ratio nodes were positioned next to the vertical isothermal surface to capture the thermal and momentum boundary layers. Vertical node refinement was used to capture the shear layers of the jet as it entered the computational domain. All computations were performed on a Macintosh II computer configured either with a MC68020 processor, or a MC68030 processor and MC68882 coprocessor. Typical CPU processing times for the latter machine were around 14 ms/time-step/cell.

The jet impingement problem was simulated with the thermal property data for two materials, glycerin and helium; and for the case of helium, four inlet jet velocities were investigated. Two thermal boundary conditions were considered for each fluid type and inlet jet velocity: 1) an isothermal surface 10°C above the inlet jet temperature and 2) a constant surface heat flux, whose value was fixed per fluid type. Although TEMPEST contains the capability for temperature dependent physical properties, the fluid properties of viscosity, thermal conductivity, specific heat, and density were fixed during the simulations. The 10 different simulations are categorized in Table 1 below; the characteristic length use in the Reynolds number was based on the diameter of the inlet jet.

TABLE 1. Simulation Parameters

No.	Fluid	Jet Reynolds No.	Prandtl No.	Thermal Boundary
1a	Glycerin	7.46×10^2	16610.	Isothermal
1b	Glycerin	7.46×10^2	16610.	Heat flux, 1300. W/m^2
2a	Helium	3.03×103	0.556	Isothermal
2b	Helium	3.03×10^3	0.556	Heat flux, 100. W/m^2
3a	Helium	3.03×10^4	0.556	Isothermal
3b	Helium	3.03×10^4	0.556	Heat flux, 100. W/m^2
4a	Helium	1.51×10^5	0.556	Isothermal
4b	Helium	1.51×10^5	0.556	Heat flux, 100. W/m^2
5a	Helium	3.03×10^5	0.556	Isothermal
5b	Helium	3.03×10^5	0.556	Heat flux, 100. W/m^2

RESULTS

Computational fluid dynamic calculations typically omit Second Law analyses because computation of entropy generation rates is not compulsory for solving the Navier-Stokes equations. The emphasis in presenting these results from the impinging jet simulations, therefore, will be concentrated on the insights afforded by

computing and visualizing local entropy generation rates. The authors note that graphics presentation of the fields of entropy generation do not translate well from the color images of a high resolution monitor to the black and white imaging of the printed page. Several approaches for performing this translation were attempted including contour plots, shaded contour plots, and photography of gray-scale images. The images that appear in this article were created by a procedure called "dither," which converts the color image into a pseudo gray-scale image through a palette of interconnected symbols. This palette, with its associated scale, is shown below each result figure that was generated through the "dither" procedure. It should be noted that the palettes are scaled differently amoung the result figures.

Space limitations prohibit the graphic presentation of the entropy generation fields for all10 of the simulations. Therefore, selected graphic results will be presented that best reveal the entropy generation characteristics. In lieu of graphic results, Table 2 below summarizes the key results from the 10 separate simulations. The second through the fourth columns in the table are the local entropy generation rates integrated over the computational domain for, contribution of entropy generation associated with viscous dissipation, thermal gradients, and combined sources, respectively. The column entitled flux represents the average surface heat flux for the thermal boundary surface. For isothermal simulations the local heat flux was a complex function of the vertical wall position, fluid properties, and jet Reynolds number, with the maximum heat fluxes occurring at the jet center line.

TABLE 2. Volume Integrated Entropy Generation Rates

No.	Viscous, W/K	Thermal, W/K	Total, W/K	Flux, W/m^2
1a	1.16	0.631	1.79	1306.4
1b	1.16	0.800×10^{-1}	1.24	1300.0
2a	0.568×10^{-5}	0.320×10^{-1}	0.320×10^{-1}	196.3
2b	0.568×10^{-5}	0.610×10^{-2}	0.611×10^{-2}	100.0
3a	0.109×10^{-2}	0.175	0.176	663.7
3b	0.109×10^{-2}	0.177×10^{-2}	0.286×10^{-2}	100.0
4a	0.134	0.348	0.482	1219.9
4b	0.134	0.758×10^{-3}	0.135	100.0
5a	0.940	0.531	1.47	1827.2
5b	0.940	0.425×10^{-3}	0.940	100.0

Two interesting features of Table 2 should be noted. The first is that for roughly equivalent average surface heat flux values (simulations 1a and 1b), the integrated entropy generation rates are lower for the constant wall heat flux. Peak local values of the entropy generation due to thermal gradients occurred in the node adjacent to the heated surface. In the case of the isothermal surface (simulation 1a), the peak value occurred at the jet center line, whereas, for the constant heat flux surface the peak value occurred at the computational domain outlet. The second interesting feature of Table 2 is again related to the difference between the isothermal and constant heat flux surface simulations. Simulations 2 through 5 were for a helium jet; where the "a"

suffix to the simulation number indicates an isothermal heated surface, and the "b" suffix indicates a constant heat flux, heated surface. For the isothermal heated surface simulations, as the jet inlet velocity increased, the total integrated entropy generation rate increased. Conversely, for the constant heat flux series of simulations a minimum in the total integrated entropy generation rate is noted for a jet inlet velocity of 10.0 m/s (simulation 3b). The increasing entropy generation rates due to viscous dissipation with increasing jet inlet speeds are offset by the decreasing entropy generation rates that result from thermal gradients. This minimum total integrated entropy generation rate was not observed in the isothermal surface simulations because the integrated surface heat transfer increased with jet speed.

The following three images (Figures 4 to 6) depict fields of local entropy generation rates for simulation 3a, separated into the viscous dissipation component, thermal gradient component, and total, respectively. The three images are equivalently scaled by the natural logarithm of the entropy generation from 4.63×10^{-9} W/K m^3 to 228.2 W/K m^3. The local entropy generation that stems from viscous dissipation (Figure 4) is concentrated in the shear layers near the jet inlet and the vertical wall boundary layers. Without the logarithm scaling of the images, the detail in the images is lost, with the perceivable entropy generation sources collapsing to the thin shear and boundary layers. The thermal gradient component of the local entropy generation rates (Figure 5), because of the logarithm scaling, appears as an enlarged boundary layer along the heated vertical surface. The relatively high entropy generation rates that occur within the entrance shear layers of the jet result from the recirculating helium at elevated temperatures mixing with the cooler inlet jet fluid. The field of total local entropy generation (Figure 6) shows the viscous dissipation component dominating the jet entrance shear region and the thermal gradient component dominating the boundary layer along the vertical heated wall. These distributions, naturally, are strongly dependent on the flow structure and thermal boundary conditions.

The fields of local entropy generation rate for the simulation with a glycerin jet with an isothermal heated surface (simulation 1a) are depicted in Figures 7 to 8. Both images in Figures 7 and 8 are scaled by the natural logarithm; however, the span of the scales differs between the two images. The field of the viscous dissipation component of local entropy generation shown in Figure 7 appears different from its counterpart for the helium jet. A significant amount of entropy generation occurs in the glycerin jet as it decelerates upon entering the computational domain. Moreover, a more equivalent distribution of viscous dissipation is occurring along the adiabatic and heated vertical surfaces. This is in contrast to the helium jet simulation where the viscous dissipation was confined to the entrance shear region and the impingement wall boundary layer. These differences in the viscous dissipation fields are attributed to the differences between jet Reynolds numbers and fluid physical properties.

An interesting estimate of numerical entropy generation may be obtained by computing the integrated thermal contribution to entropy generation for an isothermal problem. In another words, TEMPEST was executed with all of the nodes initialized with the identical temperature and all forms of internal heat generation and surface

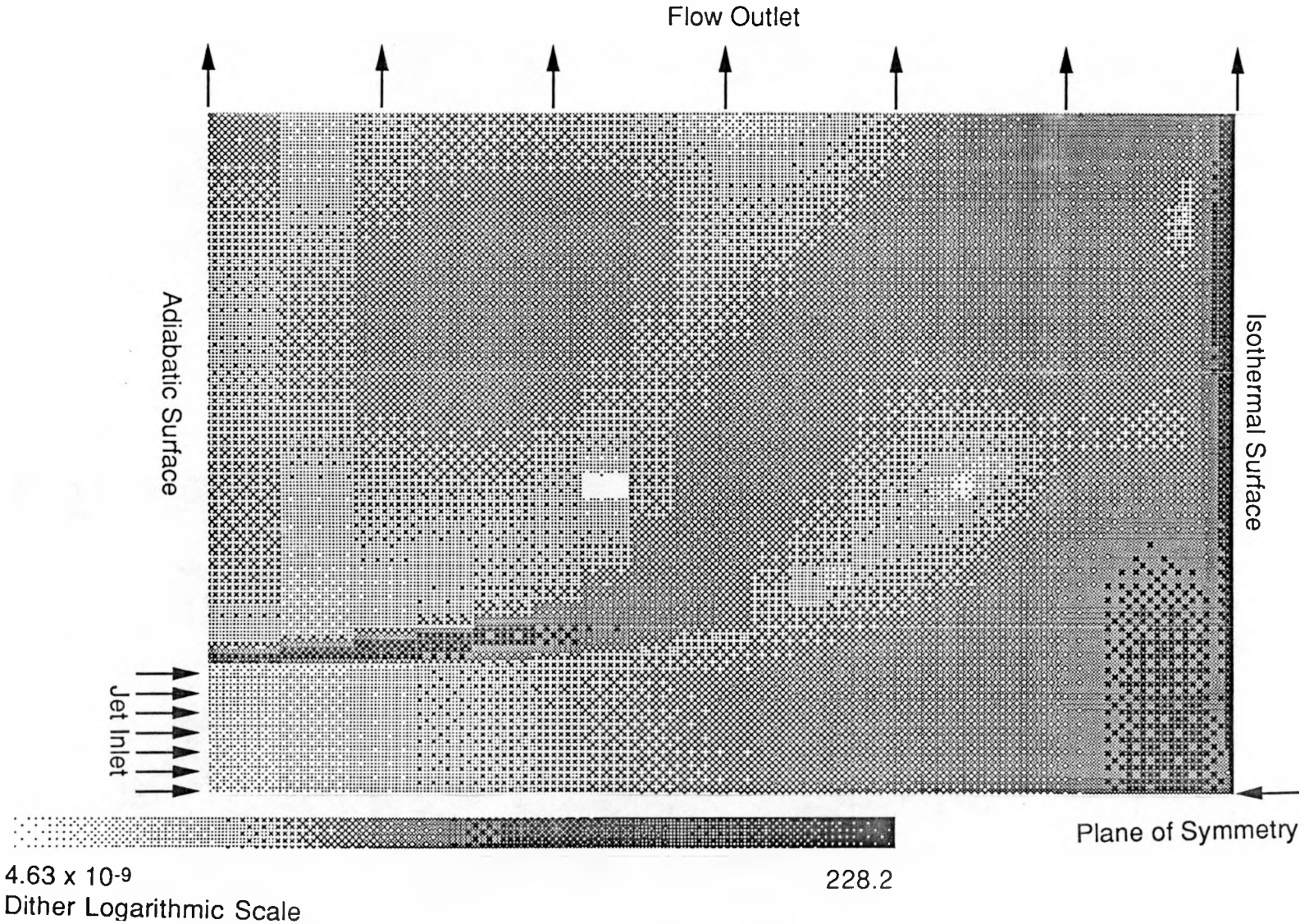

FIGURE 4. Viscous Component of Local Entropy Generation W/K m³ (No. 3a)

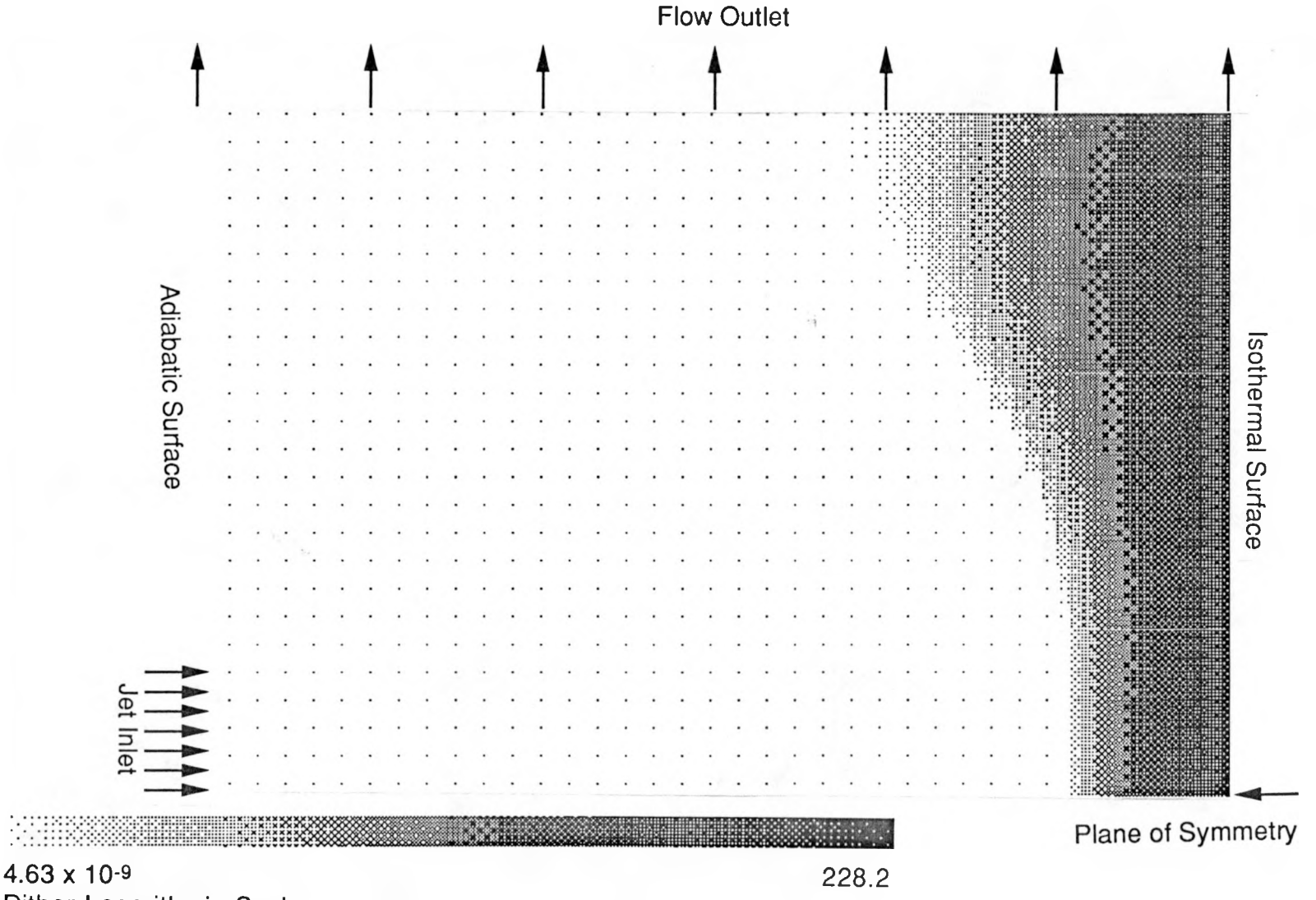

FIGURE 5. Thermal Component of Local Entropy Generation W/K m³ (No. 3a)

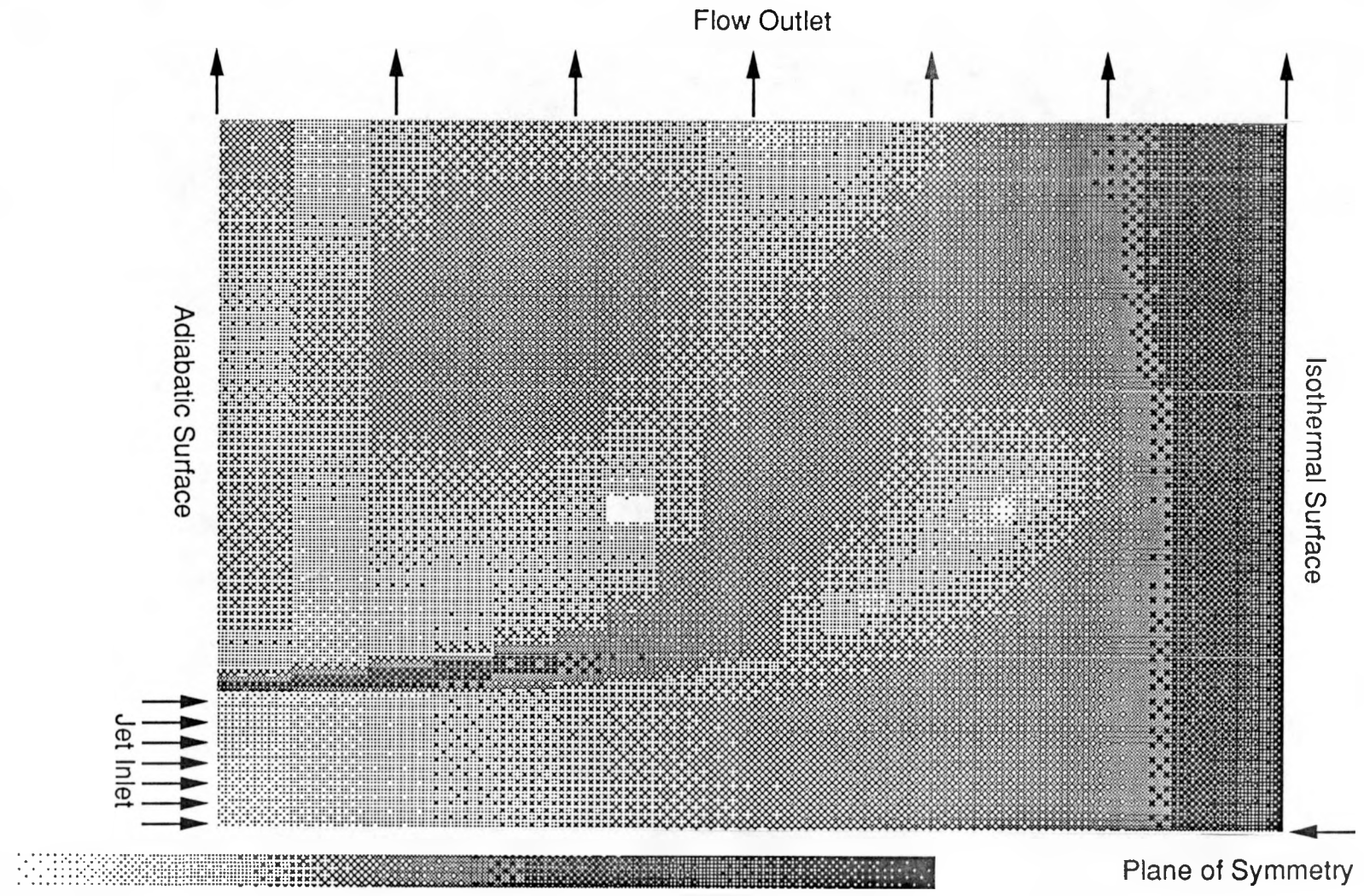

FIGURE 6. Total Local Entropy Generation W/K m3 (No. 3a)

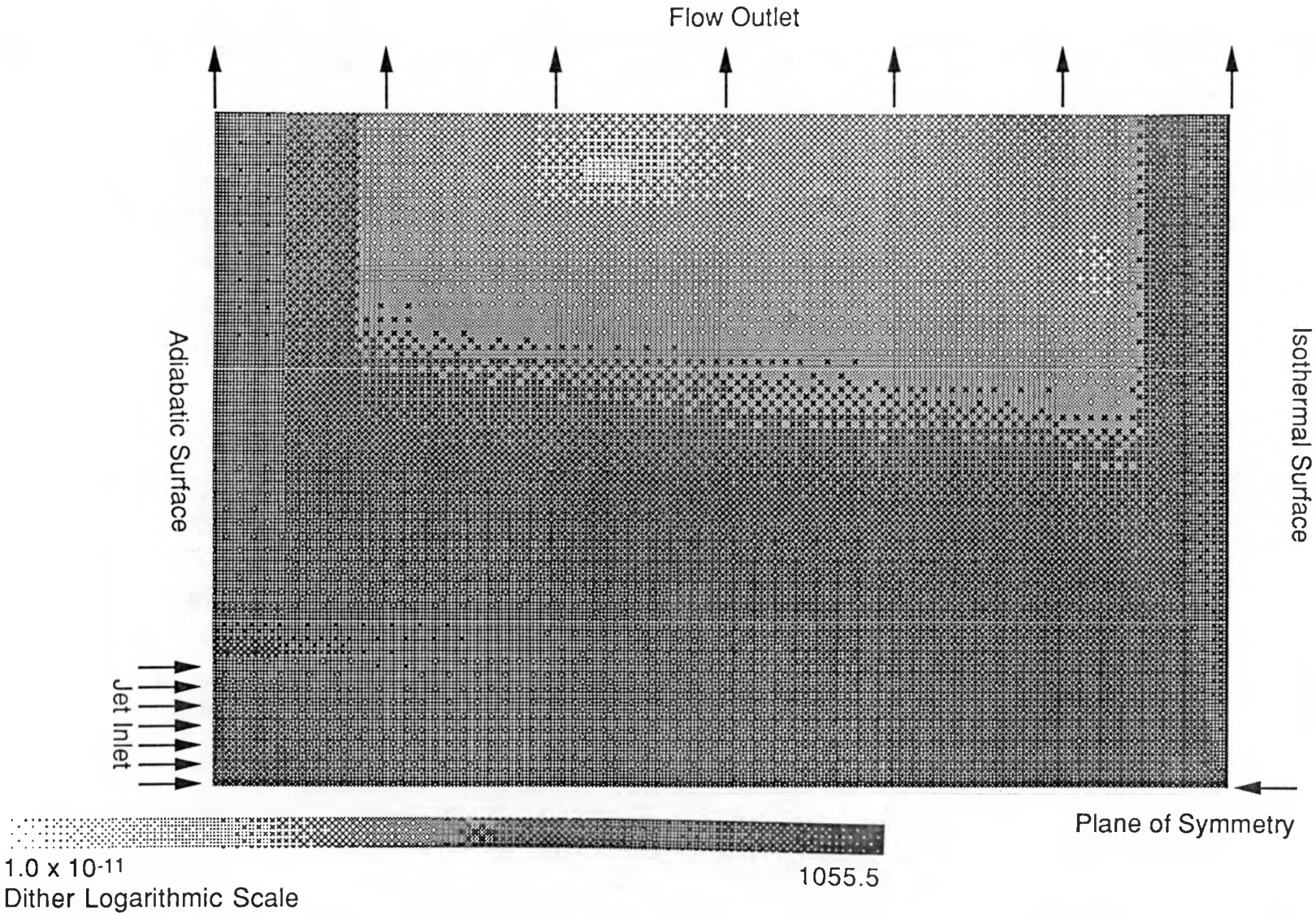

FIGURE 7. Viscous Component of Local Entropy Generation W/K m3 (No. 1a)

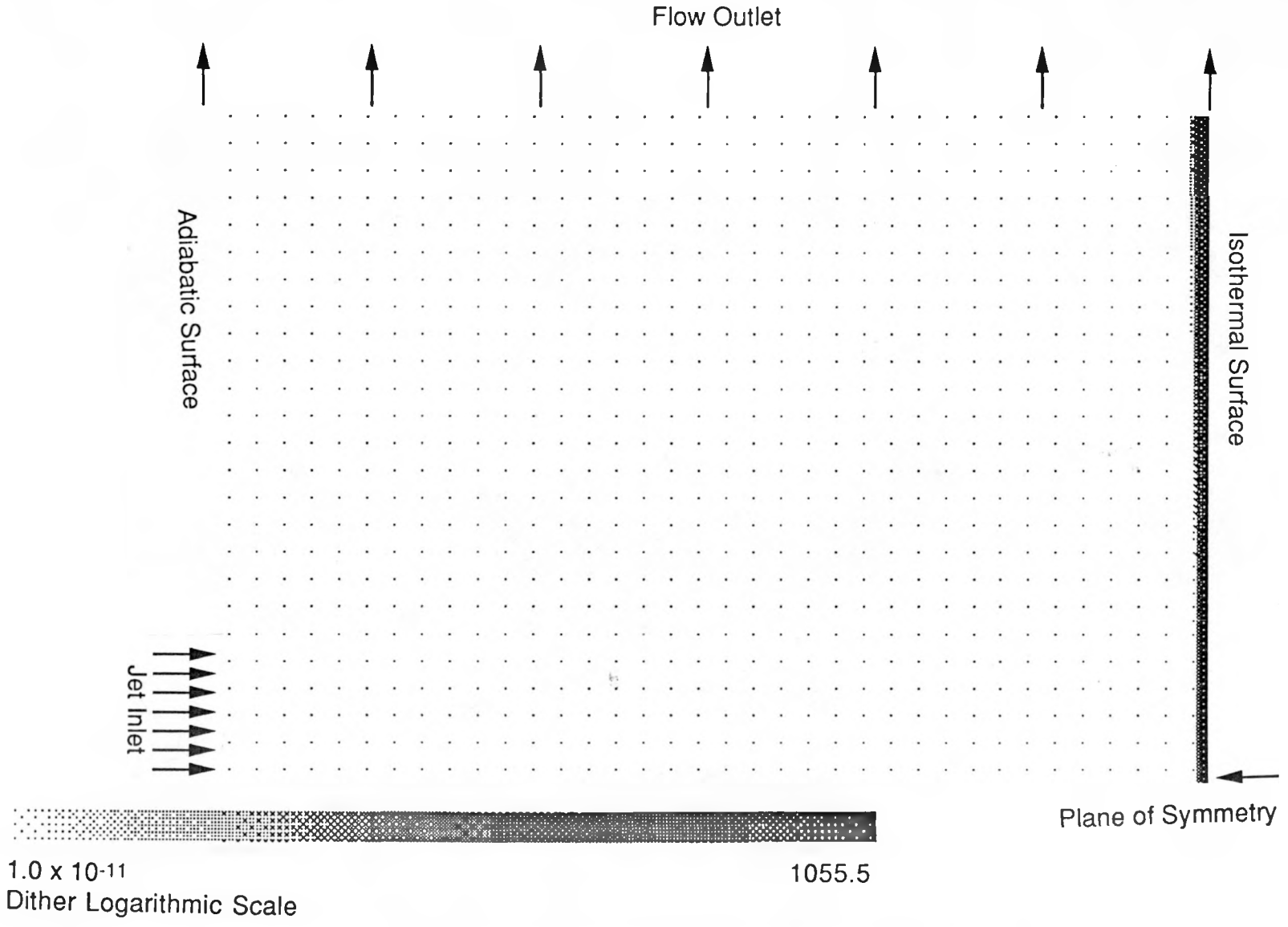

FIGURE 8. Thermal Component of Local Entropy Generation W/K m3 (No. 1a)

heat fluxes nulled, but with the energy equation being solved. The resulting temperature field was then used to compute the thermal component of entropy generation. If the simulations were completely void of numerical entropy generation then one would expect to the integrated thermal component of the entropy generation rate to equal zero. The results for these isothermal simulations, with the four helium flow fields, indicate that the numerical entropy generation levels are significantly below those of the problem; as listed in Table 3 below. The actual levels of numerical entropy generation probably do not correlate with the jet Reynolds number because the pressure convergence criterion and simulation periods differed between the simulations. The field of numerical entropy generation computed as described above for simulation number 3a is shown in Figure 9. The image indicates that the numerical entropy generation is not purely random, but rather that the regions of high flow shear and flow deceleration produce the largest entropy generation rates. These regions in the computational domain coincide with those nodes that have large aspect ratios or would improve the computational accuracy with spacing refinements.

TABLE 3. Integrated Numerical Entropy Generation Rates

No.	Jet Reynolds No.	Numerical Entropy Generation, W/K	Physical Entropy Generation, W/K
2a	3.03×10^{3}	0.240×10^{-14}	0.320×10^{-1}
3a	3.03×10^{4}	0.337×10^{-16}	0.176
4a	1.51×10^{5}	0.101×10^{-15}	0.482
5a	3.03×10^{5}	0.272×10^{-11}	0.940

ERROR ANALYSIS

An estimate of the relationship between errors in the primitive variables of temperature and velocity, and errors in the entropy generation components may be made with a few assumptions. For the viscous dissipation component, if we assume that:

$$\frac{\partial u}{\partial x} = \frac{\partial u}{\partial y} = \frac{\partial v}{\partial x} = \frac{\partial v}{\partial y}; \quad \text{and} \quad \varepsilon_u = \varepsilon_v \quad ; \tag{8}$$

then an estimate of the error in the viscous component of entropy generation that corresponds to a level error in the velocity field may be expressed as the following, for a first order finite difference scheme:

$$\varepsilon_{sgv} = 32 \frac{\mu}{T} \left\{ \frac{\varepsilon_v}{\Delta x} \frac{\Delta u}{\Delta x} + \frac{\varepsilon_v^2}{\Delta x^2} \right\} \tag{9}$$

If the velocity gradient $\Delta u/\Delta x$ is approximated by the gradient across the turbulent momentum boundary layer on the heated surface at the volume exit, Δx is approximated by the average node spacing, and the second term of Equation (9) is ignored, then a relation between an error in velocity and the viscous component of

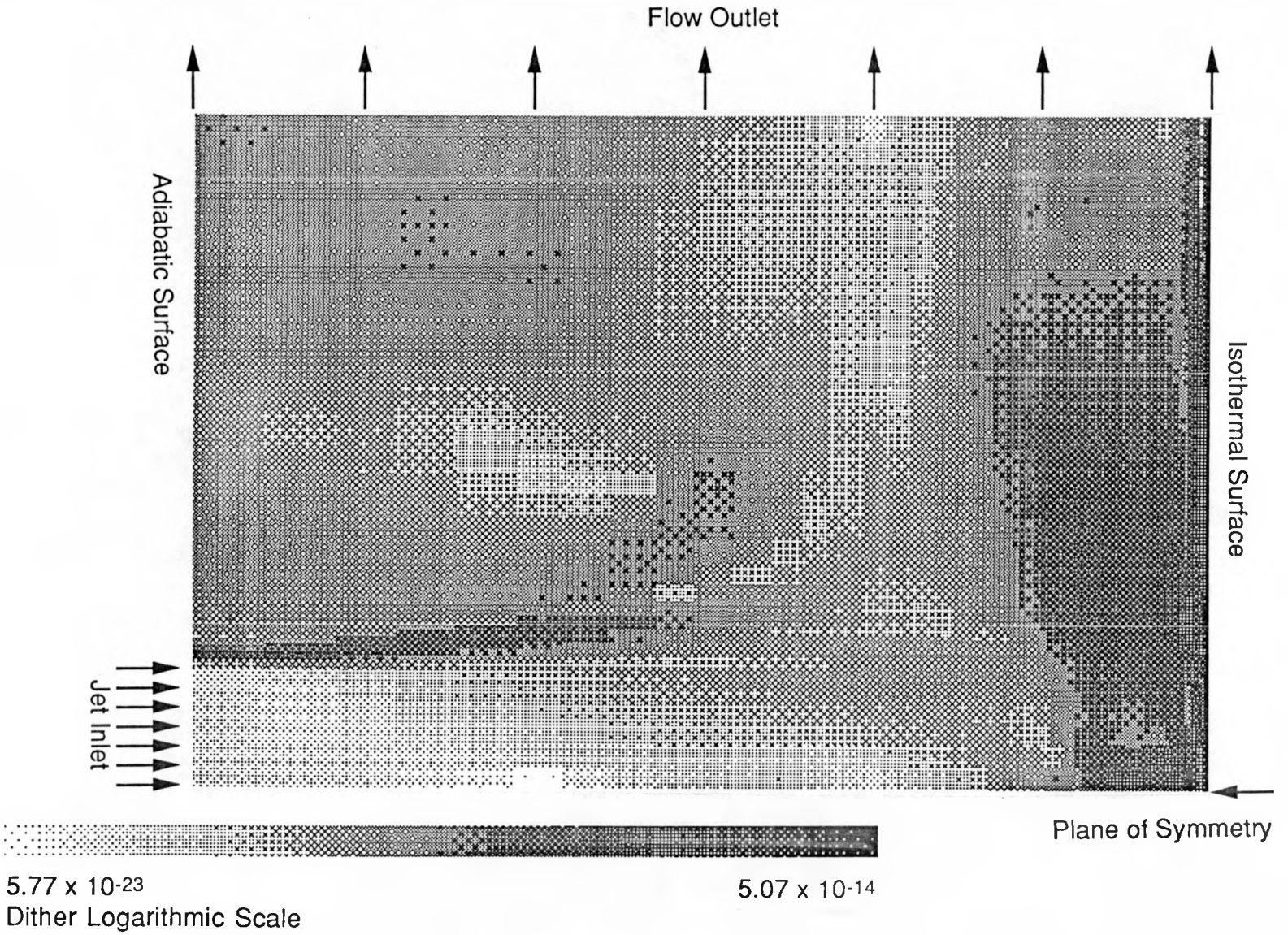

FIGURE 9. Numerical Entropy Generation W/K m3 (No. 3a)

entropy generation may be obtained. These relations are summarized in Table 4 below for the helium simulations.

A similar analysis was performed on the error in the thermal component of entropy generation with dependence on the error in the temperature field. For the thermal error analysis it was assumed that

$$\frac{\partial T}{\partial x} = \frac{\partial T}{\partial y}; \tag{10}$$

the thermal gradient $\Delta T/\Delta x$ was approximated by the gradient across the thermal boundary layer on the heated surface at the volume exit; Δx was approximated by the average node spacing; and the analogous term to the second term of Equation (9) was ignored. The relations between an error in temperature and the thermal component of entropy generation are also summarized in Table 4 below for the helium simulations.

TABLE 4. Relation Between Primitive Errors and Entropy Errors

Jet Reynolds No.	Viscous Relation	Thermal Relation
3.03×10^3	$\varepsilon_{sgv} = 2.97 \times 10^{-4}\ \varepsilon_v$	$\varepsilon_{sgt} = 5.05 \times 10^{-2}\ \varepsilon_T$
3.03×10^4	$\varepsilon_{sgv} = 4.74 \times 10^{-3}\ \varepsilon_v$	$\varepsilon_{sgt} = 8.77 \times 10^{-2}\ \varepsilon_T$
1.51×10^4	$\varepsilon_{sgv} = 3.28 \times 10^{-2}\ \varepsilon_v$	$\varepsilon_{sgt} = 1.21 \times 10^{-1}\ \varepsilon_T$
3.03×10^5	$\varepsilon_{sgv} = 7.54 \times 10^{-2}\ \varepsilon_v$	$\varepsilon_{sgt} = 1.40 \times 10^{-1}\ \varepsilon_T$

CONCLUSIONS

The results of this study confirm the feasibility and usefulness of numerical calculation of local entropy generation in complicated thermal processes. Specific conclusions concerning the feasibility of numerical calculation of local entropy generation include:

- The integration of local entropy generation calculations into an existing CFD code proved to be straightforward and did not significantly increase run time.
- The comparison of numerical and analytical results for a simple benchmarking problem was successful.
- Error analysis suggests that numerical error is very small when compared to the calculated entropy generation.

Specific conclusions concerning the usefulness of numerical calculation of local entropy generation include:

- Numerical calculations allow the investigation of the structure of local entropy generation in thermal processes. The impinging jet problem is an example. The

results show that for the sample problem, entropy generation is concentrated in the boundary layer. To a great extent, understanding the boundary layer will allow an understanding of local entropy generation. This will not necessarily be true for different geometries and more complicated processes.

- Numerical calculations can help a designer optimize a component. The results of the impinging jet problem identified a jet velocity that minimizes entropy generation. This information would be useful to a designer trying to minimize the irreversibilities in an jet impingement heat exchanger.

- Numerical calculations of local entropy generation may provide a measure of numerical entropy generation that can be compared to natural entropy generation to judge the validity of the numerical calculation.

Based on the results of this study, we have made several recommendations for future research.

- Given the simplicity and usefulness of including local entropy generation calculations in CFD codes, CFD code developers should be encouraged to incorporate local entropy generation calculation in a wide range of simulation tools.

- Local entropy generation calculations should be expanded to involve more complicated processes including multiple phases, multiple components, reacting flows, compressible flows, and radiation heat transfer.

NOMENCLATURE

c_p	specific heat, J/K kg
∂	partial derivative
Δx	node dimension in the x direction, m
ε	effective viscosity, Pa s
ε_{sgt}	error in thermal component of entropy generation, W/K m^2
ε_{sgv}	error in viscous component of entropy generation, W/K m^2
ε_T	absolute error in the temperature, K
ε_u	absolute error in the u velocity, m/s
k	thermal conductivity, W/K m
k_T	eddy thermal conductivity, W/K m
κ	effective thermal conductivity, W/K m
$\dot{q}''_o$	surface heat flux, W/m^2
r	radius, m
r_o	conduit radius, m

$\dot{S}'''_{gen}$	entropy generation rate, W/K m^2
T	temperature, K
T_o	wall temperature, K
u, v, w	x, y, z direction velocity
V	average flow velocity, m/s
μ	dynamic viscosity, Pa s
μ_T	eddy viscosity, Pa s
x, y, z	Cartesian coordinate directions

Subscripts

i	x direction node index
j	y direction node index

REFERENCES

Argrow, B.M., G Emanual, and M.L. Rasmussen. 1987. " Entropy Production in Nonsteady General Coordinates." AIAA Journal. Vol.25, No. 12.

Bejan, A. 1979a. " A Study of Entropy Generation in Fundamental Convective Heat Transfer." Journal of Heat Transfer 101:718-725

Bejan, A. 1979b. " Second Law Analysis in Heat Transfer." Presented at workshop on "The Second Law of Thermodynamics" George Washington University, Washington, D.C., August 14-16, 1979.

Bejan, A. 1982. Entropy Generation Through Heat and Fluid Flow. Wiley Interscience, New York, New York.

Drost, M.K., and J.R. Zaworski. 1988. "A Review of Second Law Analysis Techniques Applicable to Basic Thermal Science Research." In Thermodynamic Analysis of Chemically Reactive Systems. American Society of Mechanical Engineers, New York, New York.

Dunbar, W.R. 1982. Computer Simulation of a High Temperature Solid Electrolyte Fuel Cell. M. S. Thesis, Marquette University, Milwaukee, Wisconsin.

El-Sayed, Y. 1988. "On Exergy and Surface Requirements for Heat Transfer Processes Involving Binary Mixtures." In Second Law Analysis in Heat/Mass Transfer and Energy Conversion. American Society of Mechanical Engineers, New York, New York.

Hutchinson, R. A., and S.E. Lyke. 1987. "Microcomputer Analysis of Regenerative Heat Exchangers for Oscillating Flows." In Proceedings: 1987 ASME/JSME Thermal Engineering Joint Conference. Vol. 2, pp. 653. American Society of Mechanical Engineers, New York, New York.

Kays, M. W. and M. E. Crawford. 1980. Convective Heat and Mass Transfer. 2nd ed. McGraw-Hill Company, New York, New York.

Liang, H., and T.H. Kuehn. 1988. " Irreversibility Analysis of a Water to Water Mechanical Compression Heat Pump." In Analysis and Applications of Heat Pumps, American Society of Mechanical Engineers, New York, New York.

D. S. Trent, L. L. Eyler, and M. J. Budden. 1989a. TEMPEST - A Three-Dimensional Time-Dependent Computer Program for Hydrothermal Analysis, Volume 1: Numerical Methods and User Input. PNL-4348, Vol. 1, Rev. 2, Pacific Northwest Laboratory, Richland, Washington.

D. S. Trent, L. L. Eyler, and M. J. Budden. 1989b. TEMPEST - A Three-Dimensional Time-Dependent Computer Program for Hydrothermal Analysis, Volume 2: Assessment and Verification Results. PNL-4348, Vol. 2, Rev. 2, Pacific Northwest Laboratory, Richland, Washington.